PREDICTION OF BUBBLE DIAMETER AT DETACHMENT FROM A WALL ORIFICE IN LIQUID CROSS FLOW UNDER REDUCED AND NORMAL GRAVITY CONDITIONS

Henry K. Nahra*
Microgravity Science Division, Microgravity Fluid Physics Branch
NASA-John H. Glenn Research Center at Lewis Field
21000 Brookpark Rd., MS:77-5
Cleveland, OH 44135
e-mail:henry.k.nahra@grc.nasa.gov
Fax: (216) 433-8050

Y. Kamotani
Department of Mechanical & Aerospace Engineering
Case Western Reserve University
Cleveland, OH

Abstract - Bubble formation and detachment is an integral part of the two-phase flow science. The objective of the present work is to theoretically investigate the effects of liquid cross-flow velocity, gas flow rate embodied in the momentum flux force, and orifice diameter on bubble formation in a wall-bubble injection configuration. A two-dimensional one-stage theoretical model based on a global force balance on the bubble evolving from a wall orifice in a cross liquid flow is presented in this work. In this model, relevant forces acting on the evolving bubble are expressed in terms of the bubble center of mass coordinates and solved simultaneously. Relevant forces in low gravity included the momentum flux, shear-lift, surface tension, drag and inertia forces. Under normal gravity conditions, the buoyancy force, which is dominant under such conditions, can be added to the force balance. Two detachment criteria were applicable depending on the gas to liquid momentum force ratio. For low ratios,

* Corresponding author

the time when the bubble acceleration in the direction of the detachment angle is greater or equal to zero is calculated from the bubble x and y coordinates. This time is taken as the time at which all the detaching forces that are acting on the bubble are greater or equal to the attaching forces. For high gas to liquid momentum force ratios, the time at which the y coordinate less the bubble radius equals zero is calculated. The bubble diameter is evaluated at this time as the diameter at detachment from the fact that the bubble volume is simply given by the product of the gas flow rate and time elapsed. Comparison of the model's predictions was also made with predictions from a two-dimensional normal gravity model based on Kumar-Kuloor formulation and such a comparison is presented in this work.

Key Words: Force Balance, Bubble Detachment, Reduced Gravity

1. INTRODUCTION AND LITERATURE REVIEW

Several investigators have studied experimentally the process of bubble injection and detachment in still fluids under full gravity conditions. Kumar and Kuloor (1970) published an excellent review on the subject of bubble formation and detachment. They summarized the experimental work in the literature as well as the theoretical work destined to predict the bubble volume at detachment from a force balance. Marmur and Rubin (1976), modeled bubble evolution and separation in still fluid and under normal gravity condition using a force balance on elements of the interface which are expanding from balancing the surface tension and pressure forces. The work of Tan and Harris (1986) extended the work of Marmur and Rubin with the addition of the unsteady part of the potential function when solving for the liquid pressure using Bernouilli's equation. They included the effect of the gas momentum in addition to the inclusion of the gas density to allow for its increasing significance at high

system pressures. They also incorporated more refinement of the thermodynamics aspect of the problem, which involves solving for the gas flow rates and pressures of the chamber and the bubble. Kawase and Ulbrecht (1981) formulated a model based on balancing forces of the process of droplet formation and detachment from a nozzle submerged in a flowing liquid. They simulated the influence of the continuous flowing phase by virtually inclining the nozzle. Tsuge *et. al.* (1981) have investigated bubble evolution and detachment under normal garvity from an orifice submerged in a flowing liquid and studied the effects of the liquid velocity on bubble diameter. The cross liquid velocity was accounted for by the modification of the Rayleigh-Plesset (R-P) equation which describes the bubble evolution under prescribed bubble and chamber pressures. They also adopted the two-stage bubble formation and detachment process. Pinczewski (1981) developed a model for bubble formation from an orifice submerged by a liquid. The model is based on solving the modified Rayleigh equation for bubble growth in conjunction with the equation of motion for vertical translation, the orifice equation, and the chamber pressure equation. The gas momentum was accounted for by the incorporation in the modified Rayleigh equation a term that represents the pressure due to a spherical vortex. Hooper (1986) however, used the boundary element method to study the process of bubble formation at an orifice submerged in an inviscid still liquid. The flow of the surrounding liquid flow is assumed irrotational and incompressible so can be described in terms of a velocity potential, which satisfies Laplace's equation. The problem reduced to solving numerically Laplace's equation for the potential function simultaneously with the unsteady inviscid equation of motion, which relates the potential function to pressure and velocity field. Ghosh and Ulbrecht (1989) studied bubble formation from orifices submerged in a continuous phase of non-newtonian liquids under full gravity. Their theoretical model

was based on solving the pressure balance equation simultaneously with the vertical equation of motion, which is based on a force balance along the direction of bubble detachment. Zughbi *et. al.* (1984) solved the full Navier Stokes equations for a bubble forming in a fluid using the Marker-and-Cell (MAC) technique which requires extensive computing time. Unverdi and Triggvasson (1992) simulated unsteady fluid flows in which a sharp interface or a front separates fluids of different density and viscosity. The flow field is discritized by a finite difference stationary grid and the interface by a moving grid. Motion of rising bubble is simulated using their front tracking method. Marshall and Chudacek (1993) formulated a model based on a force balance to calculate the bubble detachment diameter. In their formulation, they solved simultaneously the transient chamber pressure with the orifice equation and the equation of motion in the liquid flow direction.

In low gravity, the force of buoyancy is not present, and as a result, bubbles can grow larger than the pipe or channel hydraulic diameter, thereby forming a Taylor bubble, especially when produced using smaller gas flow rates. A detaching force is needed in order to achieve bubble detachment. Bubbles can be detached by means of acoustic or electric fields, which generate a corresponding force that detach the forming bubbles. These methods are being studied by Prosperetti *et. al.* (2000) and Herman *et. al.* (2000). A fluid induced detaching force can be also considered for bubble detachment in low gravity. The cross-flow of liquid assists in the detachment process as was shown by Kim *et. al.* (1994), who developed a theoretical model based on the force balance to predict the bubble diameter at detachment from a nozzle submerged in a cross and co-flow of liquid. Direct comparison of their results with previous ground experiments showed good agreement. Tsuge *et. al.* (1997) developed a model based

on the simultaneous solution of the modified Rayleigh equation with the equation of motion using equivalent radius of curvature of the bubble gas-liquid interface. However, their model was not applicable in the cross-current configuration due to the lack of symmetry. Badalassi *et. al.* (2000) developed a 3-D code with the gas-liquid interface being captured implicitly in an Eulerian mesh. The two-phase flow was treated as a single fluid with variable properties, and with the density and viscosity changing sharply at the interfaces. Their results showed qualitative agreement with the experimental data of Misawa *et. al.* (1997). Bhunia *et. al.* (1998) revisited the co-flow calculations and reformulated the problem by including the relative velocity into the inertia term of the forming bubble. The results compared well with experimental data obtained from a low gravity nozzle-injection bubble-generation and detachment experiment performed on the NASA DC-9 Low Gravity Platform.

Bubble generation and detachment from nozzle submerged in still liquids and from wall-flush orifice injection have been studied under low gravity conditions, with and without cross liquid velocity. Pamperin and Rath, (1995) have studied the bubble formation from a submerged nozzle in a still fluid under low gravity conditions and found that detachment occurs beyond a critical Weber number where the latter is defined in terms of the gas velocity and orifice diameter. In their experimental work, they drastically reduced the buoyancy by performing the experiment in a 4.7 s drop tower. They had found experimentally that bubble detachment occurs beyond a critical Weber number ($We > 10$) in contrary to what is seen under normal gravity. They also found that a critical We (beyond which detachment occurs, i.e. $We > 8$) can theoretically be derived by balancing the momentum flux and surface tension forces. Their definition of the gas momentum flux force is reduced by a factor of 2 which increased

the theoretical We by a factor of 2. However, if the correct momentum flux force is used, then when balanced with surface tension yields the condition We > 4 as the criteria for detachment. Nahra and Kamotani (2000), in a low gravity bubble formation and detachment from a flush wall orifice experiment and under liquid cross flow, showed using a scaling analysis that when the gas momentum is large, the bubble detaches from the injection orifice as the gas momentum overcomes the attaching effects of liquid drag and inertia. The surface tension force is much reduced because a large part of the bubble pinning edge at the orifice is lost as the bubble axis is tilted by the liquid flow. When the gas momentum is small, the force balance in the liquid flow direction is important, and the bubble detaches when the bubble axis inclination exceeds a certain angle.

Emphasis on modeling of bubble detachment using force balance has not been given to the problem of wall bubble injection and detachment under conditions dominated by high momentum flux and by forces in the liquid flow direction. Wall injection of bubbles differs from bubbles formed by a nozzle submerged in a liquid cross flow setting. The differences lie in the competition of the surface tension force with other relevant forces such as the drag, shear-lift, momentum flux and inertia. It is the objective of this work to develop a global force model that predicts the bubble evolution and detachment in low gravity with considerations given to forces that are not well pronounced under normal gravity due to the masking effects of the buoyancy force.

2. CONSTANT GAS FLOW RATE MODEL

First, the assumptions that are inherent to the model are presented. This is followed by a presentation of the equation of motion for the x and y coordinates. Third, the initial conditions

relevant to the equations of motion and the detachment criteria are given. Then the results of the model are compared with the low gravity experimental results obtained by Nahra and Kamotani (2000).

2.1 Model Assumptions

The problem at hand is defined as follows. Air is injected from a flush wall orifice (inner diameter D_N) at an airflow rate of Q_g in a channel of hydraulic diameter D_P where liquid flows at a velocity U_L. The liquid flow is laminar. Basic observations made in low gravity show that the bubble tilts and detaches under different regimes of gas momentum and liquid momentum. Figure 1 illustrates the problem set-up. The assumptions for this problem are given below,

1- The liquid flow is assumed to be uniform when used in the inertia force expression and is represented by the average liquid velocity U_L. Since this model is used to compare its predictions with experimental results that were obtained on board of the NASA low gravity platform DC-9 aircraft, and since the flow of liquid is begun at every parabolic pass, the flow is determined to be unsteady. Flow velocity calculations showed the flow to be more uniform than Poiseuille-like in the channel where the bubble formation and detachment experiments were carried out.

2- Gas flow rate, Q_g, is assumed constant in time during the bubble evolution and until detachment. This is a reasonable assumption given that the density of the gas is not changing drastically between the chamber and the bubble (Hooper 1986).

3- As a consequence of the constant gas flow rate, bubble volume is assumed to evolve based on $V_B=Q_g\, t$, or $r(t)=(Qg\, t/(4/3\pi))^{1/3}$.

4- The viscous effects that are considered in this work relate to a bubble in a simple shear flow and not a bubble evolving from and attached to a wall at the orifice interface.

2.2 Equation of Motion in the x Direction

The important forces in the x-direction are the inertia which can be attaching or detaching depending on the sign of the relative velocity between the evolving bubble and the liquid, the surface tension which is attaching and the drag which is a detaching force.

2.2.1 Inertia Force

The inertia force is obtained from the decomposition of Eq. 1 (given below) into an x and y coordinates. Equation 1 is given by, (Bhunia *et. al.*, 1998),

$$\vec{F}_I = \frac{d}{dt}\left(\rho_g V_B \frac{d\vec{S}}{dt}\right) + \frac{d}{dt}\left[\rho_L C_M V_B \left(\frac{d\vec{S}}{dt} - U_L \hat{i}\right)\right] \quad \text{.....(1)}$$

We let the x-component of **S** be x(t) and similarly, the y-component be y(t). Moreover, we substitute $Q_g\, t$ for V_B. Then, the x-component inertia force becomes,

$$F_{Ix} = Q_g\left(-C_M U_L \rho_L + (\rho_g + C_M \rho_L)x'(t) + t(\rho_g + C_M \rho_L)x''(t)\right) \quad \text{.....(2)}$$

2.2.2 Drag Coefficient and Drag Force

Drag force and C_D, the drag coefficient are given by,

$$F_{Dx} = \frac{1}{2} C_D \rho_L \pi r^2 \sqrt{(U_L - x')^2 + y'^2}\,(U_L - x') \cdots\cdots (a);$$
$$C_D = \frac{15.34}{Re_B} + \frac{2.163}{Re_B^{0.6}} \cdots\cdots (b) \qquad \text{.....(3)}$$

Re_B is the bubble Reynolds number defined as $D_B U_L/\nu$. The drag coefficient was obtained from a numerical calculation performed by Legendre and Magnaudet, 1998, where the drag coefficient on a bubble in a simple shear was calculated as well as the shear lift coefficient. The tabulated data for the drag coefficient in the work of Legendre and Magnaudet were fitted into Eq. 3 (b).

2.2.3 Surface Tension Force

The surface tension force $F_{\sigma x}$ is calculated by integrating the attaching surface tension force components (that point in the negative x and y direction) over the orifice rim. The x-component of the surface tension force points in the negative x direction and is given by,

$$F_{\sigma x} = 2\int_{\frac{\pi}{2}}^{3\frac{\pi}{2}} D_N \sigma Cos[\gamma(\phi)] Sin(\phi) d\phi \qquad \text{.....(4)}$$

The relation between γ the bubble interface local inclination angle and ϕ the longitudinal angle is given by,

$$\gamma(\phi) = (a\phi^2 + b\phi + c)\hat{H}_{Unit\,Step}(\phi - \phi_0) + \beta \hat{H}_{Unit\,Step}(\phi_0 - \phi) \qquad \text{.....(5)}$$

In Eq. 5, $\hat{H}_{Unit\ Step}$ is the Heavyside unit step function, the constants a, b, and c are determined from the values of α and β shown in Fig. 1, and the angle ϕ_0 is the onset of the quadratic transition from β to α. The surface tension force in the x-direction is calculated as a function

of the inclination angle θ by numerical integration of Eq. 4 for three different nozzle diameters, D_N=0.033, 0.076 and 0.15 cm. The results are fitted into quadratic equations and are shown below:

$$F_{\alpha\beta}[\theta, D_N] = \begin{cases} +0.240\theta - 0.130\theta^2 \rightarrow D_N = 0.033cm \\ +0.555\theta - 0.300\theta^2 \rightarrow D_N = 0.076cm \\ +1.095\theta - 0.593\theta^2 \rightarrow D_N = 0.15cm \end{cases} \quad \text{.....(6)}$$

In these equations θ is taken as $\tan^{-1}(x/y)$. Equation 6 describes the integrated surface tension of a bubble that is being formed from a wall orifice with two different interface angles α and β, and an inclination angle θ. It reflects the current experimental observations that were made in low gravity where the bubble does not develop a neck. Therefore Eq. 6 was used into the model. After the introduction of the forces in the x-direction, the force balance results in,

$$Q_g\left(-C_M U_L \rho_L + \left(\rho_g + C_M \rho_L\right)x'(t) + t\left(\rho_g + C_M \rho_L\right)x''(t)\right) =$$

$$\frac{1}{2}C_D \rho_L \pi r^2 \sqrt{\left(U_L - x'\right)^2 + y'^2}\left(U_L - x'\right) - \quad \text{.....(7)}$$

$$\begin{cases} +0.240\theta - 0.130\theta^2 \rightarrow D_N = 0.033cm \\ +0.555\theta - 0.300\theta^2 \rightarrow D_N = 0.076cm \\ +1.095\theta - 0.593\theta^2 \rightarrow D_N = 0.15cm \end{cases}$$

2.3 Equation of Motion in the y-Direction

The force balance in the y direction represents a competition between the detaching and attaching forces acting on the forming bubble. The detaching forces (pointing in the +y direction, Fig. 1) are the buoyancy, shear lift, momentum flux, and pressure. The attaching forces are the surface tension and the drag.

2.3.1 Inertia Force

Application of Eq. 1 to the y-component yields the following:

$$F_{Iy} = Q_g\left(\left(\rho_g + C_M\rho_L\right)y'(t) + t\left(\rho_g + C_M\rho_L\right)y''(t)\right) \quad \text{.....(8)}$$

It can be noted that the inertia force in the y direction does not involve U_L that came from the relative velocity term of the inertia illustrated in Eq. 1.

2.3.2 Drag

The drag force in y direction differs from the x-component drag force by the exclusion of the relative velocity effect because to the liquid velocity is along the x direction (y' *vs.* U_L-x'). Using the same drag coefficient as in Eq. 3, the drag force becomes,

$$F_{Dy} = \frac{1}{2}C_D\rho_L\pi r^2\sqrt{(U_L - x')^2 + y'^2}\,y' \quad \text{.....(9)}$$

2.3.3 Surface Tension Force

The surface tension y-component points in the negative y direction and is given by:

$$F_{\sigma y} = 2\int_{\frac{\pi}{2}}^{3\frac{\pi}{2}} D_N\sigma Sin[\gamma(\phi)]d\phi \quad \text{.....(10)}$$

The $\gamma(\phi)$ function described in Eq. 5 is used without changing the parameter ϕ_0. Integration of Eq. 10 for different orifice diameter as a function of the inclination angle θ and fitting the results in quadratic equation in θ yield:

$$F_{\sigma y}[\theta, D_N] = \begin{cases} 5.15 - 5.25\theta - 1.33\theta^2 \rightarrow D_N = 0.033cm \\ 11.8 - 12.1\theta - 3.08\theta^2 \rightarrow D_N = 0.076cm \\ 23.4 - 23.9\theta - 6.08\theta^2 \rightarrow D_N = 0.15cm \end{cases} \quad \text{.....(11)}$$

Equation 11 was used to calculate the surface tension force components in the y-direction with $\theta = tan^{-1}(x/y)$. The use of Eq. 11 is justified by the same argument made in the previous section.

2.3.4 Shear Lift Force

The shear lift force used in this model is given by the following:

$$F_{SLy} = \frac{1}{2} C_L \rho_L \pi r^2 U_l^{\,2} \quad \text{.....(12)}$$

For intermediate Re_B, Legendre and Magnaudet (1998) calculated the following relation for the shear lift coefficient,

$$C_L^{high\,Re} = \frac{1}{2} \frac{1 + 16\,Re_B^{-1}}{1 + 29\,Re_B^{-1}} \cdots\cdots 5 < Re_B < 500 \quad \text{.....(13)}$$

As can be seen, Eq. 13 shows no dependence on the dimensionless shear rate. The shear lift force becomes important in low gravity because of the absence of the buoyancy force acting on the bubble. This force on a bubble of 3 mm in diameter can be up to 5 % of the buoyancy force. Figure 2 shows the lift to drag coefficient as calculated from Eqs. 3b and 13. For bubble Reynolds numbers above ~60, we see that the lift coefficient is greater than the drag coefficient. Since the prevailing bubble Reynolds numbers are in the range shown in Fig. 2,

one can deduce that in low gravity, the shear lift force is an important force to be included in the force balance.

The shear lift and drag forces acting on the bubble represent the forces induced by the stress tensor on the bubble surface. These forces are connected with a bubble that is positioned in a simple shear flow and away from any wall. It is suggested that the existence of a surface near the bubble changes the flow field and creates a high-pressure region near the wall. The existence of the wall becomes apparent in the situation where there is a cross flow of liquid over the bubble.

2.3.5 Pressure Force

The pressure force consists of two components. The first component is attributed to the difference in pressure between the gas at the orifice tip and the liquid pressure. The second component is attributed to the contact pressure (Klausner/Shyy, 1999) at y = 0. These two components may explain the aforementioned compromise/reduction of the surface tension force that attaches the bubble to the orifice rim (Nahra and Kamotani, 2000). The pressure force is given by the following,

$$\vec{F}_P = \left(\left(\frac{2\sigma}{r_B} \right) \frac{\pi}{4} D_N{}^2 + F_{CP} \right) \hat{j} \qquad \text{.....(14)}$$

$$F_{CP} = \pi \sigma R_N \mathrm{H}_{Unit\,Step}(t, U_L)$$

Here $2\sigma/r$, the first component of the pressure force, is the interfacial tension pressure (Klausner/Shyy et. al., 1999) and F_{CP} is contact pressure force at y = 0. The force $(2\sigma/r)\,\pi\,R_N^2$ represents the net pressure force acting on the bubble control volume. It also can be interpreted as reaction force acting on the bubble control volume. The contact pressure force,

F_{CP} which scales as ~ $\pi\sigma R_N \hat{H}_{Unit\ Step}(t, U_L)$ may also be attributed physically to the effects of near-stagnation point(s) around the bubble base where the flow slows down and a high-pressure region is created that results in stretching of the interface and consequently helps the bubble detachment. Here $\hat{H}_{Unit\ Step}(t, U_L)$ is the unit step Heavyside function. This force acts in the positive y direction and is classified as a detaching force whose direct effect is the reduction or compromise of the surface tension force.

2.3.6 Momentum

The momentum flux force is given by the following,

$$\bar{F}_M = \iint_{S_N} \bar{V}\left(\rho \bar{V} \cdot d\bar{A}\right) = \rho V_g{}^2 A\hat{j} = \rho_g \frac{Q_g^2}{\pi/4 D_N^2} \hat{j} \quad \text{.....(15)}$$

This is a detaching force and is rather relevant with smaller orifice diameters that result in greater gas velocities.

Combination of all the above expressions into one equation yields the force balance equation in the y coordinate,

$$Q_g\left(\left(\rho_g + C_M\rho_L\right)y'(t) + t\left(\rho_g + C_M\rho_L\right)y''(t)\right) =$$

$$\underbrace{-\frac{1}{2}C_D\rho_L\pi r^2\sqrt{\left(U_L - x'\right)^2 + y'^2}\,y'}_{Drag}$$

$$+\underbrace{\frac{4}{3}\pi r^3 g\left(\rho_L - \rho_g\right)}_{Buoyancy} + \underbrace{\frac{1}{2}\rho_L U_L{}^2\pi r^2 C_L}_{Shear-Lift} + \underbrace{\frac{4\rho_g Q_g{}^2}{\pi D_N{}^2}}_{Momentum-Flux} + \qquad \text{.....(16)}$$

$$\underbrace{\left(\left[\frac{2\sigma}{r}\right]\frac{\pi}{4}D_N{}^2 + F_{CP}\right)}_{Pressure} - \underbrace{\begin{cases} 5.15 - 5.25\theta - 1.33\theta^2 \rightarrow D_N = 0.033cm \\ 11.8 - 12.1\theta - 3.08\theta^2 \rightarrow D_N = 0.076cm \\ 23.4 - 23.9\theta - 6.08\theta^2 \rightarrow D_N = 0.15cm \end{cases}}_{Surface\ Tension}$$

2.4 Bubble Diameter at Detachment

Equations 7 and 16 are solved simultaneously in order to calculate the bubble diameter at detachment. In order to perform the calculation, first we substitute for r(t),

$$r(t) = \left(\frac{Q_g t + V_{B0}}{4/3\,\pi}\right)^{\frac{1}{3}} \qquad \text{.....(17)}$$

where V_{B0} is the volume of a hemisphere of radius $D_N/2$. Substitution of the various forces into the force model results in the following set of equations:

$$Q_g\left(-C_M U_L \rho_L + \left(\rho_g + C_M \rho_L\right)x'(t) + t\left(\rho_g + C_M \rho_L\right)x''(t)\right) =$$

$$\underbrace{\frac{1}{2}\left(\frac{15.34}{\left(\frac{Q_g t + V_{B0}}{4/3\pi}\right)^{\frac{1}{3}} 2U_L/\nu} + \frac{2.16}{\left(\left(\frac{Q_g t + V_{B0}}{4/3\pi}\right)^{\frac{1}{3}} 2U_L/\nu\right)^{0.6}}\right) \times \pi\rho_L\left(\frac{Q_g t + V_{B0}}{4/3\pi}\right)^{\frac{2}{3}} \sqrt{\left(U_L - x'\right)^2 + y'^2}\left(U_L - x'\right)}_{Drag}$$

$$-\underbrace{\begin{cases} +0.240\theta - 0.130\theta^2 \rightarrow D_N = 0.033cm \\ +0.555\theta - 0.300\theta^2 \rightarrow D_N = 0.076cm \\ +1.095\theta - 0.593\theta^2 \rightarrow D_N = 0.15cm \end{cases}}_{Surface\ Tension} \qquad \text{.....(18)}$$

$$Q_g\left(\left(\rho_g + C_M\rho_L\right)y'(t) + t\left(\rho_g + C_M\rho_L\right)y''(t)\right) =$$

$$\underbrace{-\frac{1}{2}\left(\frac{15.34}{\left(\frac{Q_g t + V_{B0}}{4/3\pi}\right)^{\frac{1}{3}} 2U_L/\nu} + \frac{2.16}{\left(\left(\frac{Q_g t + V_{B0}}{4/3\pi}\right)^{\frac{1}{3}} 2U_L/\nu\right)^{0.6}}\right)\pi\rho_L\left(\frac{Q_g t + V_{B0}}{4/3\pi}\right)^{\frac{2}{3}}\sqrt{\left(U_L - x'\right)^2 + y'^2}\,y'}_{Drag}$$

$$+\underbrace{\frac{4}{3}\pi r^3 g\left(\rho_L - \rho_g\right)}_{Buoyancy} + \underbrace{\frac{4\rho_g Q_g^{\,2}}{\pi D_N^{\,2}}}_{Momentum-Flux} +$$

$$\underbrace{\frac{1}{2}\rho_L U_L^{\,2}\pi\left(\frac{Q_g t + V_{B0}}{4/3\pi}\right)^{\frac{2}{3}}\frac{1}{2}\frac{1 + 16\dfrac{\nu}{\left(\frac{Q_g t + V_{B0}}{4/3\pi}\right)^{\frac{1}{3}} 2U_L}}{1 + 29\dfrac{\nu}{\left(\frac{Q_g t + V_{B0}}{4/3\pi}\right)^{\frac{1}{3}} 2U_L}} + \left(\left[\frac{2\sigma}{\left(\frac{Q_g t + V_{B0}}{4/3\pi}\right)^{\frac{1}{3}}}\right]\frac{\pi}{4}D_N^{\,2} + F_{CP}\right)}_{Shear-Lift\ \&\ Pressure} - \underbrace{\begin{cases} 5.15 - 5.25\theta - 1.33\theta^2 \rightarrow D_N = 0.033cm \\ 11.8 - 12.1\theta - 3.08\theta^2 \rightarrow D_N = 0.076cm \\ 23.4 - 23.9\theta - 6.08\theta^2 \rightarrow D_N = 0.15cm \end{cases}}_{Surface\ Tension}$$

.....(19)

The variables that are solved for are x(t) and y(t). The initial conditions are as follows:

$$\begin{aligned} &x'(0) = x(0) = 0; \\ &y'(0) = 0;\ y(0) = 0 \end{aligned} \quad \text{.....(20)}$$

2.4.1 Detachment Criteria

It was shown by Pamperin and Rath (1995) that under no cross flow conditions, bubble detachment in low gravity is primarily governed by the balance between the gas momentum

and surface tension forces. If the momentum force is significantly less than the surface tension, detachment does not occur, and the opposite is true. If the ratio of the two forces is set to be ≥ 1, such a ratio reduces to a Weber number that is based on the gas velocity U_g and the orifice diameter D_N. We show this as follows:

$$\frac{\left|\vec{F}_M\right|}{\left|\vec{F}_\sigma\right|} = \frac{4\rho_g Q_g^{\,2}/\pi D_N^{\,2}}{\pi\sigma D_N} = \frac{1}{4}\frac{16\rho_g Q_g^{\,2}}{\pi^2\sigma D_N^{\,3}} \geq 1 \Rightarrow We = \frac{16\rho_g Q_g^{\,2}}{\pi^2\sigma D_N^{\,3}} \geq 4 \quad \text{.....(21)}$$

As previously mentioned, the definition of the momentum force in Pamperin and Rath's work is one half the momentum force shown above in Eq. 21. This changes the condition above to,

$$\frac{\left|\vec{F}_M\right|}{\left|\vec{F}_\sigma\right|} = \frac{2\rho_g Q_g^{\,2}/\pi D_N^{\,2}}{\pi\sigma D_N} = \frac{1}{8}\frac{16\rho_g Q_g^{\,2}}{\pi^2\sigma D_N^{\,3}} \geq 1 \Rightarrow We = \frac{16\rho_g Q_g^{\,2}}{\pi^2\sigma D_N^{\,3}} \geq 8 \quad \text{.....(22)}$$

Their experimental results show that no detachment occurred in the 4.7 s low gravity period for We ≤ 10. For cases where the We ≥ 10, detachment occurred and the dimensionless bubble diameter decreased with We.

The detachment criteria for the cross flow problem at hand is proposed based on the competition between the liquid and gas momentum forces per unit area. For gas to liquid momentum force ratio ≤ 1 and for a ratio of gas flow rate to critical gas flow rate $Q_g/Q_{gCrit\mu g}$ < 0.15, or equivalently We < 0.6, the detachment criterion is defined as the time at which the detaching forces exceed the attaching ones and thereby the acceleration in the direction of detachment becomes positive. Here the low gravity critical gas flow rate $Q_{gCrit\mu g}$ from Pamperin and Rath (1995) is simply obtained by setting the gas Weber number equal to the

limiting We for detachment, i.e. We = 4 for the theoretical limit. The criterion $Q_g/Q_{gCrit\mu g} <$ 0.15, or equivalently We < 0.6 was obtained numerically from running the relevant cases and determining the cut-off line that separates this regime from the one dominated by the momentum force. In order to formulate the detachment criterion, the acceleration components in the x and y directions were projected on the detachment angle of inclination. The acceleration and detachment criterion in such a direction becomes,

$$a(t) = \cos\left(\tan^{-1}\frac{x(t)}{y(t)}\right)y''(t) + \sin\left(\tan^{-1}\frac{x(t)}{y(t)}\right)x''(t) \geq 0 \quad \text{.....(23)}$$

The root of this equation is the time of detachment t_d of the bubble that is under a set of detaching forces that have overcome the attaching forces. This criterion is applied primarily for the bubbles made from D_N=0.076 and 0.15 cm where such condition was true. This is in concert with the experimental observations made by Nahra and Kamotani (2000), regarding these two diameters and the bubbles they produced under the cross flow conditions at hand. As was suggested by Nahra and Kamotani (2000), forces in the x direction were as important as in the y direction in the determination of the bubble diameter at detachment unlike bubbles produced from D_N=0.033 cm where the momentum force of the gas was predominant. For this case, bubbles were produced as if normal gravity conditions were present in the process due to the strength of the momentum flux force. This regime resembles the regime given by Pamperin and Rath (1995) except for the fact that there is a cross flow of liquid. For the regime where the gas momentum to liquid momentum force ratio is greater than 1, and $Q_g/Q_{gCrit\mu g} > 0.15$, or equivalently We > 0.6, the proposed detachment criterion is similar to the one used by Kumar and Kuloor (1970) except for the neck length taken as zero. This is in

concert as well with the observation made by Nahra and Kamotani (2000) where scaling showed that the dimensionless bubble diameter in this regime is based on a balance of forces in the y direction. Therefore, the detachment criterion being similar to Kumar-Kuloor's criterion is justified based on the experimental observations. A summary of the detachment criteria is given by,

$$For\ \frac{\rho_g U_g^{\ 2}}{\rho_L U_L^{\ 2}} \geq 1,\ and\ \frac{Q_g}{Q_{gCrit|\mu g}} \geq 0.15\ or\ We \geq 0.6, \rightarrow y(t) - r(t) \geq 0$$

$$For\ \frac{\rho_g U_g^{\ 2}}{\rho_L U_L^{\ 2}} < 1,\ and\ \frac{Q_g}{Q_{gCrit|\mu g}} < 0.15\ or\ We < 0.6, \rightarrow a(t) \geq 0; \qquad \text{.....(24)}$$

$$a(t) = cos\left(tan^{-1}\frac{x(t)}{y(t)}\right)y''(t) + sin\left(tan^{-1}\frac{x(t)}{y(t)}\right)x''(t)$$

In order to execute detachment criteria calculations, interpolating functions for $y - r = 0$ and $a(t) = 0$ were generated in Mathematica®™ from the solutions x(t) and y(t). The roots of these functions represented by Eq. 24 were found using the bisection method written in Mathematica®™. The bubble diameter is then determined from r(t) by:

$$D_B = 2\left(\frac{Q_g t_d + V_{B0}}{4/3\pi}\right)^{\frac{1}{3}} \qquad \text{.....(25)}$$

Three Mathematica®™ notebooks (one for each orifice diameter) were written in order to perform the calculations for the bubble detachment. The difference between these notebooks is the orifice diameter, the gas flow rate pertinent to the experimental conditions of each of the orifices, the surface tension functions described above for different orifice diameters and the appropriate detachment criterion.

3. MODEL RESULTS-LOW GRAVITY

3.1 Comparison of Predicted and Experimental Results

In this section, the model's predictions are compared with the experimental results obtained from a bubble formation and detachment experiment carried out on board of the NASA DC-9 low gravity platform. During this experiment, bubbles were injected from a wall orifice into a liquid cross flow. Three orifice diameters (D_N=0.033, 0.076, and 0.15 cm) wee used for bubble injection. The air flow rate Q_g ranged from 0.7 to 1.3 cm^3/s for D_N=0.033 cm, 0.3 to 1 cm^3/s for D_N=0.076 cm, and 0.02 to 0.22 cm^3/s for D_N=0.15 cm. The liquid velocity U_L was varied from 2 cm/s to 14 cm/s. Bubble diameter at detachment was measured as a function of the liquid velocity and gas flow rate. In these low gravity experiments, two regimes of bubble formation were identified. The first is momentum flux dominated whereas in the second regime, forces in the direction of flow were relevant and their balance proved important to explain the experimental trends (Nahra and Kamotani, 2000). The motion in the z-direction was not considered because the motions in the x and y directions were deemed to be dominant. Experimentally, the bubble motion in the z direction was not measured or even observed because of the lack of cameras that could have been used to observe such a motion. G-jitter existed in all directions in the airplane but no appreciable effect of the g-jitter was observed in the bubble motion. Therefore, we concluded that g-jitter in the z-direction did not affect the main bubble motion.

3.1.1 Predicted Bubble Kinematics and Detachment Criteria

We present in this section the trends the model predicts for the variables that compose the detachment criteria, namely, the y(t) and r(t) for the detachment criterion $y - r \geq 0$ and for $a(t) \geq 0$. Figure 3 and Fig. 4 show the calculated y(t) and r(t) coordinates of a typical run for

Q_g=0.92 cm^3/s, and D_N=0.033 cm in low gravity with the following parameters, U_L=2.59 cm/s (Fig. 3), and U_L=12 cm/s (Fig. 4). We see from these figures that as the liquid velocity is increased, the intersection of the y and r curves occurred sooner which signifies a smaller bubble diameter with increased liquid cross velocity. Figure 5 and Fig. 6 show the same plots for normal gravity with the same parameters as the previous two figures. It is clearly apparent that the difference in the time of detachment is significantly less as the velocity is increased from 2.59 cm/s to 12 cm/s.

The model at hand does not capture all the details of neck formation and bubble detachment due to the collapsing of the neck because this is a global force model. However, this experimental feature is reflected in the prediction through the behavior of the y coordinate under the change of the liquid velocity and the calculation of the time to detachment from the intersection of y and r. Under normal gravity conditions, the y coordinate is not very sensitive to changing the liquid velocity due to the strong effect of the buoyancy force. Figure 7 shows the predicted bubble acceleration as a function of time for Q_g=0.7 cm^3/s, U_L=5 cm/s and 10 cm/s. The upper-dashed (lower-solid) curve corresponds to the higher (lower) liquid velocity. This trend is proper because the longer detachment time t_d results in the larger bubble diameter observed at the lower liquid velocity.

3.1.2 Bubble Diameter at Detachment-Effects of Liquid Velocity

Figures 8, 9, and 10 show the predicted and experimental bubble diameter at detachment as a function of the average cross liquid velocity for the parameters shown in the figures. In Fig. 8 and 9, the flow rate of gas was taken as the middle of the range of gas flow rates realized in the experiments using D_N=0.033 and 0.076 cm because the bubble diameter was rather

independent of the gas flow rate. For the largest orifice diameter, it was observed experimentally that the bubble diameter depended on the gas flow rate. For this reason, Fig. 10 shows the bubble diameter as a function of liquid cross velocity for two-gas flow rates, 0.02 and 0.2 cm^3/s. We see that the model predicts the experimental data in low gravity reasonably well especially for the larger orifice diameters. The maximum relative difference between the experimentally measured and predicted bubble diameter at detachment (i.e $\left|\left(D_{B\,Pred.} - D_{B\,Exp.}\right)/D_{B\,Pred.}\right|$) is 23% for D_N=0.033 cm, 12% for D_N=0.076 cm and 8% for D_N=0.15 cm for Qg=0.2 cm^3/s. It is worth noting that the model detachment criterion is not based on any empirical or semi empirical correlation that describes the detachment process, unlike the ones reported in the literature for global force models. Detachment is determined from the acceleration in the detachment direction being greater or equal to 0 or from the time when $y - r \sim 0$.

3.1.3 Bubble Diameter at Detachment-Effects of Gas Flow Rate

The effects of the gas flow rate on the bubble diameter are explored further for the case of D_N=0.15 cm where the bubble diameter was shown experimentally to increase with increasing gas flow rate. Figure 11 shows the predicted and measured bubble diameter plotted as a function of the gas flow rate. Two cases are plotted. The first of which corresponded to U_L=13.2 and the second to 5.2 cm/s. The trends show a reasonable agreement between the predicted and measured bubble diameters at detachment. The maximum relative difference between the experimentally measured and predicted bubble diameter at detachment is 18 %. Figure 12 shows the experimental and predicted bubble diameter plotted as a function of the gas flow rate for two cases of liquid velocity, U_L=2.6 and 5.5 cm/s and for D_N=0.033 cm. The

scale on the bubble diameter (0-15 mm) is considered similar to other figures for the purpose of consistency. The experimental part of this plot shows the weak dependence of the bubble diameter on the gas flow rate and the predicted part assures this behavior. The cross liquid velocity plays an important role in establishing this behavior. Here, the maximum relative difference between the experimentally measured and predicted bubble diameter at detachment is 25%. If the liquid velocity is not present, the bubble diameter is shown by Pamperin and Rath (1995) to decrease with gas flow rate in the regime of gas Weber number where detachment occurs (i.e. We > 4 (10)) due to the strength of the momentum force. Given the gas flow rates at hand, the calculated Weber number is definitely less than the theoretical (experimental) value of 4 (10). This leads one to deduce that the liquid velocity has a significant effect on the bubble detachment because even at lower liquid velocities, the forming bubble still detaches.

3.1.4 Bubble Diameter at Detachment-Effects of Liquid Surface Tension Coefficient

This calculation was performed in order to assess the effects of water contamination on the bubble diameter through the changes in the surface tension coefficient. Figure 13 shows the effects of changing the surface tension coefficient on the predicted bubble diameter as a function of the cross liquid velocity. Predicted and experimental bubble diameter at detachment as a function of average cross liquid velocity are shown for two values of the surface tension coefficient, namely, σ = 60 dynes/cm (lower curve) and 70 dynes/cm (upper curve) and for D_N=0.15 cm are shown in Fig. 13. It is clear from the plot that as σ decreases, the surface tension force decreases and the effect of surface tension in keeping the bubble attached to the surface decreases as well. This makes the time to detachment smaller, thereby resulting in smaller diameter bubbles. It is worthy to note that the two curves envelop that

experimental data. The surface tension coefficient was not measured prior and after the experiment. However, since we started with pure distilled and not de-ionized water, we believe that the inherent contaminants acquired from the experiment compromised the water surface tension coefficient. This suggests that the surface tension coefficient was less than 70 dynes/cm which corresponds to the surface tension of pure de-ionized water.

3.2.5 Bubble Diameter at Detachment-Effect of gravity levels

In order to assess the effects of gravity on the bubble diameter, the bubble diameter at detachment D_B was plotted in Fig. 14 as a function of the gravity levels g/g_0 for D_N=0.033 cm and for U_L = 1 cm/s. As expected, the bubble diameter at detachment decreases with increasing gravity level due to the increase in buoyancy which as g approaches g_0=980 cm/s^2, the buoyancy force becomes the most important detaching force that results in bubble detachment. The reason for choosing D_N=0.033 cm case was that given the range of gas flow rates and liquid velocities, the same detachment criterion ($y - r \sim 0$) can be used in low and normal gravity cases. Under full gravity, the relevance of $\pi\sigma R_N \hat{H}_{UnitStep}(t, U_L)$ becomes lesser due to the dominance of the gravity and its consequences of creating the buoyancy force on the detaching bubble.

4. MODEL RESULTS-NORMAL GRAVITY

In this work, prediction of the bubble diameter at detachment under normal gravity conditions is accomplished using the existing model adopted for normal gravity and using Kuamr-Kuloor model modified for a two dimensional geometry.

4.1 Current Model Modified for Normal Gravity

Figure 15 shows the predicted and measured bubble diameter at detachment as a function of the cross liquid velocity using the current model adapted for normal gravity condition by changing the gravity level and the detachment criterion from $y - r \sim 0$ to $y - r - R_N \sim 0$. The gas flow rates and the liquid velocity range are similar for those in low gravity. This change in the detachment criterion is adopted in order to account for the formation of the bubble neck under normal gravity conditions.

The effect of adding or deleting F_{CP} on the bubble diameter at detachment under full gravity is found to be negligible. This is in agreement with the physical situation at hand. The reason is that under normal gravity conditions, the buoyancy force dominates the process of detachment. Such a force is far stronger in 1-g, which makes the forming bubble lifts upward and thereby forms a neck that pins the bubble to the orifice diameter. Since the bubble is well pinned by the dynamics of force interactions, the loss of pinning is not present and deletion of such a force is justified. Moreover, since F_{CP} may be attributed to the loss of pinning and compromises the surface tension-attaching force, it is seen that the role of such a force is negligible in normal gravity because buoyancy lifts the bubble up and causes its pinning to the orifice diameter.

4.2 Details of Kumar-Kuloor Model Modified to Two Dimensions

This model is based on the fact that the bubble experiences two stages in its development. The first that is called the expansion phase ends at a point in time where the forces acting on the bubble are in equilibrium. When this is true, the equations of motion can be solved and a critical radius, r_{fbe}, can be calculated at the end of this phase. The bubble velocity and traveled

distance at this moment in time can serve as the initial conditions for the second phase of bubble life designated by the detachment phase. The detachment phase ends when the vertical displacement of the bubble center of mass is comparable to the bubble radius at the end of the expansion phase, r_{fbe}. During this phase, the equations of motion for the bubble are solved simultaneously in a coupled fashion as in the microgravity model. The x and y coordinates are allowed to evolve until the bubble neck length equals the critical radius determined at the end of the expansion phase. Mathematically, this translates to,

$$\sqrt{x^2(t)+y^2(t)}-r(t)=S(t)-r(t)\geq r_{fbe} \quad \text{.....(26)}$$

where $S(t)$ is the magnitude of the vector position of the bubble center of mass and r_{fbe} is the critical bubble radius determined at the end of the expansion phase. Results of predictions using this model are shown in Fig. 15 for both orifice diameters D_N=0.033 and 0.076 cm and for a range of gas flow rates that is similar to the low gravity experiment. We see from Fig. 15 that the two models are in reasonable agreement. This two stage model, although gives a reasonable comparison with the experimental results without using any adjustable parameters fails in predicting the low gravity behavior. The concept of using two-stage model is not relevant to low gravity because the lack of buoyancy precludes the development of a bubble neck as seen from the experimental results. Therefore, the one-stage model is more relevant to low gravity than normal gravity.

In addition, we show in Fig. 15 the limiting bubble diameter as $U_L \rightarrow 0$ under the governing gas flow rates experienced in the experiment. According to Oguz and Prosperetti (1993), there are critical gas flow rates below which the bubble diameter follows the quasi-static regime, tends

to be constant with gas flow rate, and follows the Fritz formula which is basically a balance between the buoyancy and surface tension force and which is given by,

$$D_F = 2\left(3\sigma D_N / 4\rho g\right)^{1/3} \quad \text{.....(27)}$$

The critical gas flow rate in normal gravity $Q_{gCritlNg}$ as calculated by Oguz and Prosperetti is given by,

$$Q_{gCrit|Ng} = \pi\left(\frac{16}{3g^2}\right)^{1/6}\left(\frac{\sigma D_N}{2\rho}\right)^{5/6} \quad \text{.....(28)}$$

Based on Eq. 28, the critical flow rates for D_N=0.033 and 0.076 are 0.45 and 0.93 cm^3/s. For the smaller orifice diameter, the critical flow rate is less than the gas flow rates we have measured in the experiment. Therefore, the bubble diameter becomes a function of the flow rate and such dependency is given by (Oguz and Prosperetti, 1993),

$$D_B = 2\left(\frac{9Q_g^{\,2}}{8\pi^2 g}\right)^{1/5} \quad \text{.....(29)}$$

Application of Eq. 29 to our experiment gives a bubble diameter of 0.326 cm or 3.26 mm at U_L=0 and Q_g = 1 cm^3/s and for the orifice D_N=0.033 cm. For D_N=0.076, and for Q_g = 0.7 cm^3/s that is below 0.93 cm^3/s, use of the Fritz formula yields a bubble diameter of D_B=3.19 mm and that is less than the bubble diameter obtained for D_N=0.033 cm. For a gas flow rate Q_g = 1.1 cm^3/s which is greater than the critical gas flow rate of 0.93 cm^3/s, the bubble diameter as calculated from Eq. 29 becomes 3.4 mm. Another limiting bubble diameter is also shown in Fig. 15 for D_N=0.15 cm (with $Q_{gCritlNg}$ = 1.7 cm^3/s) and for $Q_g < Q_{gCritlNg}$ and Q_g

$> Q_{gCritlNg}$. For $Q_g < Q_{gCritlNg}$, the limiting bubble diameter is about 4 mm. However, for $Q_g > Q_{gCritlNg}$, the limiting bubble diameter becomes a function of the flow rate and is 5 mm for a gas flow rate $Q_g = 3$ cm^3/s. These approximations made by Oguz and Prosperetti were based on simple force models that did not take into effect all the forces acting on the bubble as did the model by Kumar and Kuloor. These calculated bubble diameters are shown also on Fig. 15.

5. CONCLUDING REMARKS

In this work, a global force model for prediction of bubble diameter at detachment in low gravity was described and its predictions were compared with the experimental results obtained in low gravity on board of the NASA DC-9 low-gravity platform. This model was extended for normal gravity condition and its predictions were compared with the experimental results obtained under normal gravity. The latter predictions were also compared with the predictions of the Kumar-Kuloor approach that was based on the two-stage model.

The model can be applied to cross flow cases of higher liquid velocities and different gas flow rates. The bubble Reynolds number, Re_B should be between 5 and 500 because the shear lift force calculation is based on this criterion. The bubble diameters predicted by this model are less than ½ the hydraulic diameter of the channel. Detachment of large bubbles (on the order of Taylor bubble) cannot be predicted by this model because of the calculation of viscous forces which should be modified accordingly, in addition to the significant bubble deformation which must be taken into consideration. Bubble deformation is reflected in the bubble Weber number which should be less than or on the order of 1 in order for the nearly

spherical bubble growth to apply. Detachment of significantly deformed bubbles cannot be predicted by this model because of the inherent assumption of spherical bubble growth.

Predictions of the global force model compared well with the experimental results reported by Nahra and Kamotani, 2000. However, a more rigorous approach to this problem requires numerical methods and CFD in order to better understand the pressure distribution around the evolving bubble and the treatment of its moving interface. A more rigorous approach would also encompass the accurate evaluation of the drag and shear lift coefficient based on the computed stresses on the bubble. Moreover, the lift force is expected to be higher for the pinned evolving bubble than that for a bubble in a simple shear flow because of the existence of the wall and the stagnation point(s) associated with the pinned bubble. The drag coefficient is expected to be different from the one used because of the deviation from spherical bubbles and the mere existence of the wall. These important factors can only be, without any idealization of the flow, evaluated numerically and it is recommended their assessment be carried out in such a manner.

ACKNOWLEDGEMENTS

The work performed at Case Western Reserve University is supported by NASA under Grant NAG3-1913.

NOTATION

a(t)	*Bubble acceleration (cm/s^2)*
a,b,c	*Constants determined from the bubble angles α and β*
C_D	*Drag coefficient*
C_L	*Lift coefficient*
C_M	*Added mass coefficient*
D_B	*Bubble diameter (cm)*
D_N	*Diameter of injection orifice (cm)*
D_p	*Channel hydraulic diameter or pipe diameter (cm)*
F_B	*Buoyancy force (dynes)*
F_D	*Drag force (dynes)*
F_I	*Inertia force (dynes)*
F_{SL}	*Shear lift force (dynes)*
F_M	*Momentum flux force (dynes)*
F_σ	*Surface tension force (dynes)*
g	*Gravitational acceleration (cm/s^2)*
$\hat{H}$	*Heavyside unit step function*
$\hat{\imath}$	*Unit vector in the x direction*
$\hat{\jmath}$	*Unit vector in the y direction*
Q_g	*Gas, dispersed phase-air flow rate (cm^3/s)*
r	*Bubble radius as a function of time (cm)*
r_{fbe}	*Bubble radius at end of expansion phase (cm)*
Re_B	*Reynolds number based on bubble diameter*
S	*Position vector for the bubble center of mass (cm)*
S_N	*Surface are of orifice (cm^2)*
t	*Time (s)*
U_L	*Average superficial liquid velocity (cm/s)*
V_g	*Gas velocity from orifice (cm/s)*
V_B	*Bubble volume (cm^3)*
We	*Weber number*
x	*Component of motion along the x axis (cm)*
y	*Component of motion along the y axis (cm)*

Subscripts

B	*Bubble*
C	*Chamber*
CritlNg	*Critical based on normal gravity conditions*
Critlμg	*Critical based on microgravity or low gravity conditions*
d	*Detachment*
F	*Fritz*
g	*Disperse phase-Gas*
L	*Continuous phase-Liquid, Lift*
N	*Orifice*
P	*Channel or pipe*

SL	*Shear lift*
Unit Step	*Unit step function*
x,y	*Rectangular coordinates*
0	*Reference*

Superscripts

high Re	*High Reynolds Number*
+	*Slightly greater than zero*

Greek Symbols

α	*Frontal bubble contact angle*
β	*Back bubble contact angle*
ϕ	*Longitudinal angle (degrees, radians)*
π	*Constant*
θ	*Bubble inclination angle (degrees or radians)*
γ	*Local contact angle function*
ρ	*Density (g/cm^3)*
ν	*Kinematic viscosity (cm^2/s)*
σ	*Surface Tension Coefficient (dynes/cm)*

Mathematical Symbols

$\int$	*Integral*
‘	*First time derivative*
“	*Second time derivative*

Acronyms

CFD	*Computational Fluid Dynamics*
NASA-GRC	*National Aeronautics and Space Administration-Glenn Research Center*

REFERENCES

Badalassi, V.;Takahira, H.; Banerjee, S., "Numerical simulation of three dimensional bubble growth and detachment in a microgravity shear flow," Fifth Microgravity Fluid Physics and Transport Phenomena Conference, Cleveland, OH, August 2000.

Bhunia, A.; Pais, S.; Kamotani, Y.; Kim, I. "Bubble formation in a coflow configuration in normal and reduced gravity," *AIChE Journal*, **44** (1998) 1499-1507.

Ghosh, A.K.; Ulbrecht, J.J. "Bubble Formation from a Sparger in Polymer Solution-I. Stagnant Liquid," *Chem. Eng. Science,* **44** No. 4 (1989) 957-968

Herman, C. "Experimental Investigation of Pool Boiling Heat Transfer Enhancement in Microgravity in the Presence of Electric Fields," Fifth Microgravity Fluid Physics and Transport Phenomena Conference, Cleveland, OH, August 2000.

Hooper, A.P. "A Study of Bubble Formation at a Submerged Orifice Using Boundary Element Method," *Chem. Eng. Science,* **41** (1986) 1879-1890

Kawase, Y.; Ulbrecht, J. J. "Formation of drops and bubbles in flowing liquids," *Ind. Eng. Chem. Process Des. Dev.,* **20** (1981) 636-640.

Kim, I.; Kamotani, Y.; and Ostrach, S. "Modeling of bubble and drop formation in flowing liquids in Microgravity," *AIChE Journal* **40**, (1994) 19-28.

Kumar, R.; Kuloor, N. R. "The formation of bubbles and drops", *Advances in Chemical Engineering* **8**, (1970) 256-365.

Legendre, D.; Magnaudet, J. "The Lift Force on a Spherical Bubble in a Viscous Linear Shear Flow," *J. Fluid Mech,* **368** (1998) 81-126.

Marmur, A.; Rubin, E. A "Theoretical Model for Bubble Formation at an Orifice Submerged in an Inviscid Liquid," *Chem. Eng. Sci.,* **31** (1976) 453-463

Marshall, S.H.; Chudacek, M.W. "A model for bubble formation from an orifice with liquid cross flow," *Chem. Engn. Science,* **11** (1993) 2049-2059.

Misawa, M. *et.al* "Bubble growth and Detachment in Shear Flow Under Microgravity Conditions," *Experimental Heat Transfer, Fluid Mechanics and Thermodynamics,* Ed, Giot M *et.al.* 1997, 987-994

Nahra, H.K.; Kamotani, Y. "Bubble Formation from Wall Orifice in Liquid Cross-Flow under Low Gravity," *Chem. Engn. Sci.,* **55** (2000) 4653-4665

Oguz, H.N.; Prosperetti, A. "Dynamics of Bubble Growth and Detachment from a Needle," *J. Fluid Mech,* **257** (1993) 111-145

Pamperin, O.; Rath, H. "Influence of buoyancy on bubble formation at submerged orifices," *Chem. Engng. Sci.,* **50** (1995) 3009-3024.

Pinczewski, W.V. "The Formation and Growth of Bubbles at a Submerged Orifice," *Chem. Engn. Sci.,* **36** (1981) 405-411.

Prosperetti, A.; Hao, Y.; Oguz, H.N. "Pressure Radiation Forces on Vapor Bubbles," Fifth Microgravity Fluid Physics and Transport Phenomena Conference, Cleveland, OH, August 2000.

Shyy, W.; Narayan, R. *Fluid Dynamics at Interfaces,* Cambridge University Press, 1999.

Tan, R.B.H.; Harris, I.J. "A Model for Non-Spherical Bubble Growth at a Single Orifice," *Chem. Eng. Sci.,* **41** (1986) 3175-3182.

Tsuge, H.; Hibino, S.; Nojima, U. "Volume of a bubble formed at a single submerged orifice in a flowing liquid," *International Chemical Engineering* **21**, (1981) 630-636.

Tsuge, H.; Tanaka, Y.; Terasaka, K.; and Matsue, H. "Bubble formation in flowing liquid under reduced gravity," *Chem. Engng. Science* **52**, (1997) 3671-3676.

Unverdi, S. O., Tryggvason, G., "A Front Tracking Method for Viscous, Incompressible, Multi-Fluid Flows", *J. Computational Physics,* **100**, (1992) 25-37.

Zughbi, H. D., Pinczewski W. V. and Fell, C. J., "Bubble Growth by the Cell and Marker Technique", 8th Aust. Fluid Mech. Conf., 8B. 9-8B.12, 1984.

FIGURES LEGEND

Figure 1. Bubble coordinates and problem geometry. Note the forces acting on the bubble in the x and y directions.

Figure 2. Ratio of the Lift to Drag coefficient as a function of the bubble Reynolds number

Figure 3. Predicted r(t) [solid] and y(t) [dashed] as a function of time up to the detachment point for the following conditions, D_N=0.033 cm, Q_g=0.92 cm^3/s, U_L=2.59 cm/s, and low gravity conditions.

Figure 4. Predicted r(t) [solid] and y(t) [dashed] as a function of time up to the detachment point for the following conditions, D_N=0.033 cm, Q_g=0.92 cm^3/s, U_L=12 cm/s, and low gravity conditions.

Figure 5. Predicted r(t) and y(t) as a function of time up to the detachment point for the following conditions, D_N=0.033 cm, Q_g=0.92 cm^3/s, U_L=2.59 cm/s, and normal gravity conditions.

Figure 6. Predicted r(t) and y(t) as a function of time up to the detachment point for the following conditions, D_N=0.033 cm, Q_g=0.92 cm^3/s, U_L=12 cm/s, and normal gravity conditions.

Figure 7. Bubble acceleration as a function of time up to the detachment point for Q_g=0.2 cm^3/s, U_L=5 cm/s (solid curve) and 10 cm/s (dashed curve), and D_N=0.15 cm. Note that the shorter time to detachment corresponds to a higher liquid velocity.

Figure 8. Bubble diameter at detachment as a function of the cross liquid velocity for D_N=0.033 cm and Q_g=0.92 cm^3/s.

Figure 9. Bubble diameter at detachment as a function of the cross liquid velocity for D_N=0.076 cm and Q_g=0.7 cm^3/s.

Figure 10. Bubble diameter at detachment as a function of the cross liquid velocity for D_N=0.15 cm and Q_g=0.2 and 0.02 cm^3/s.

Figure 11. Bubble diameter at detachment as a function of gas flow rate for D_N=0.15 cm and U_L=13.2 and 5.2 cm/s. The lower set of data points corresponds to U_L=13.2 cm/s.

Figure 12. Bubble diameter at detachment as a function of gas flow rate for D_N=0.033 cm and U_L=2.9 and 5.5 cm/s

Figure 13. Predicted effects of the surface tension coefficient on the bubble diameter at detachment for D_N=0.15 cm.

Figure 14. Bubble diameter as a function of the gravity levels for D_N=0.033 cm, Q_g=0.92 cm^3/s, and U_L=1 cm/s.

Figure 15. Predicted and experimental bubble diameter at detachment for normal gravity condition.

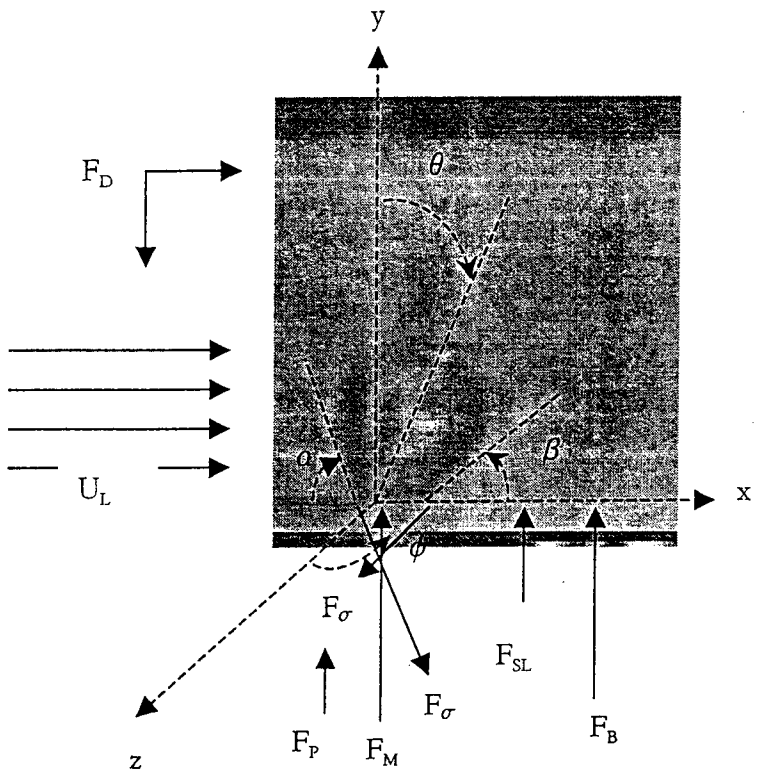

Figure 1. Bubble coordinates and problem geometry. Note the forces acting on the bubble in the x and y directions.

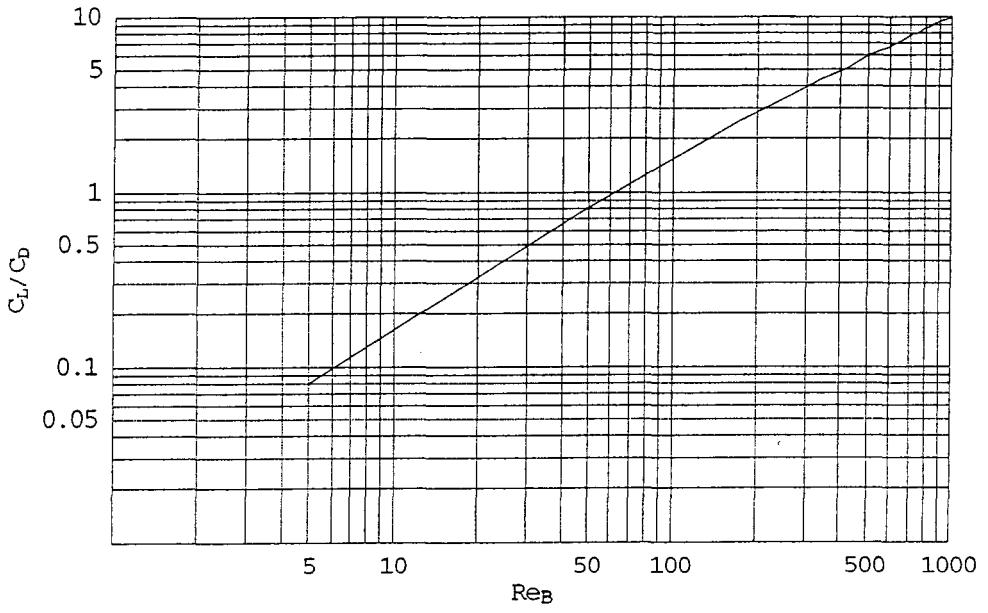

Figure 2. Ratio of the Lift to Drag coefficient as a function of the bubble Reynolds number

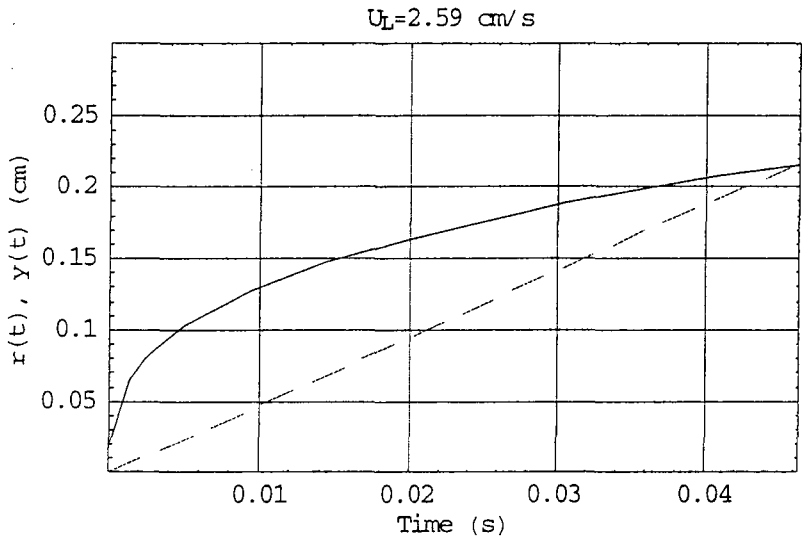

Figure 3. Predicted r(t) [solid] and y(t) [dashed] as a function of time up to the detachment point for the following conditions, D_N=0.033 cm, Q_g=0.92 cm^3/s, U_L=2.59 cm/s, and low gravity conditions.

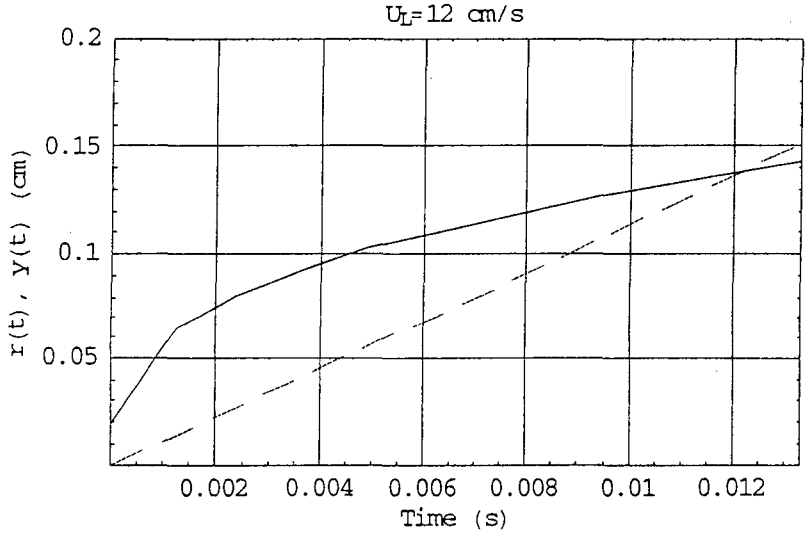

Figure 4. Predicted r(t) [solid] and y(t) [dashed] as a function of time up to the detachment point for the following conditions, D_N=0.033 cm, Q_g=0.92 cm^3/s, U_L=12 cm/s, and low gravity conditions.

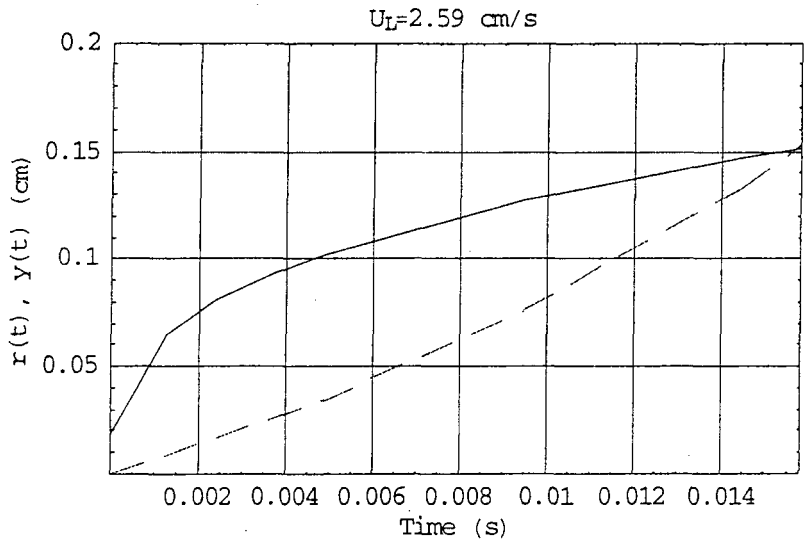

Figure 5. Predicted r(t) [solid] and y(t) [dashed] as a function of time up to the detachment point for the following conditions, D_N=0.033 cm, Q_g=0.92 cm^3/s, U_L=2.59 cm/s, and normal gravity conditions.

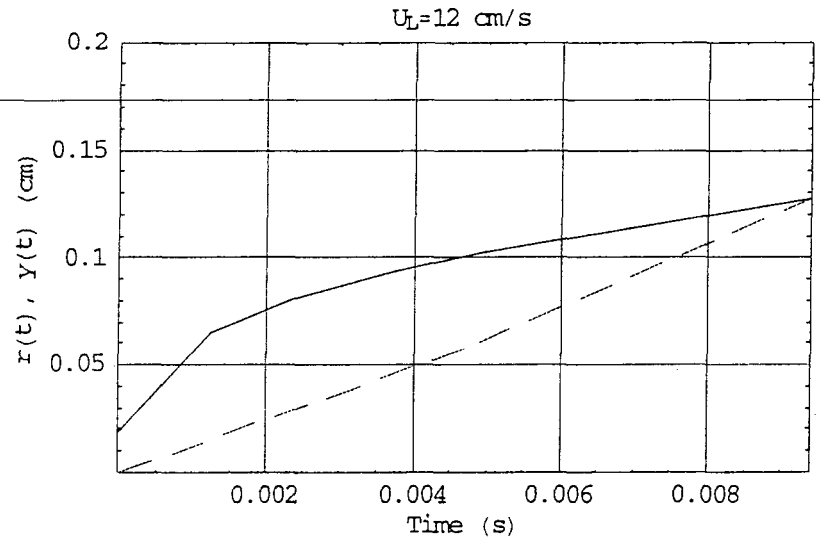

Figure 6. Predicted r(t) [solid] and y(t) [dashed] as a function of time up to the detachment point for the following conditions, D_N=0.033 cm, Q_g=0.92 cm^3/s, U_L=12 cm/s, and normal gravity conditions.

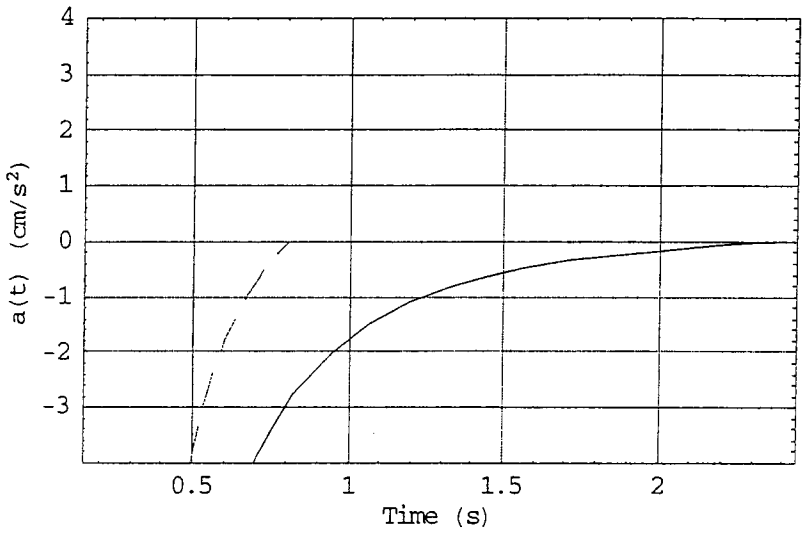

Figure 7. Bubble acceleration as a function of time up to the detachment point for Q_g=0.2 cm^3/s, U_L=5 cm/s (solid curve) and 10 cm/s (dashed curve), and D_N=0.15 cm. Note that the shorter time to detachment corresponds to a higher liquid velocity.

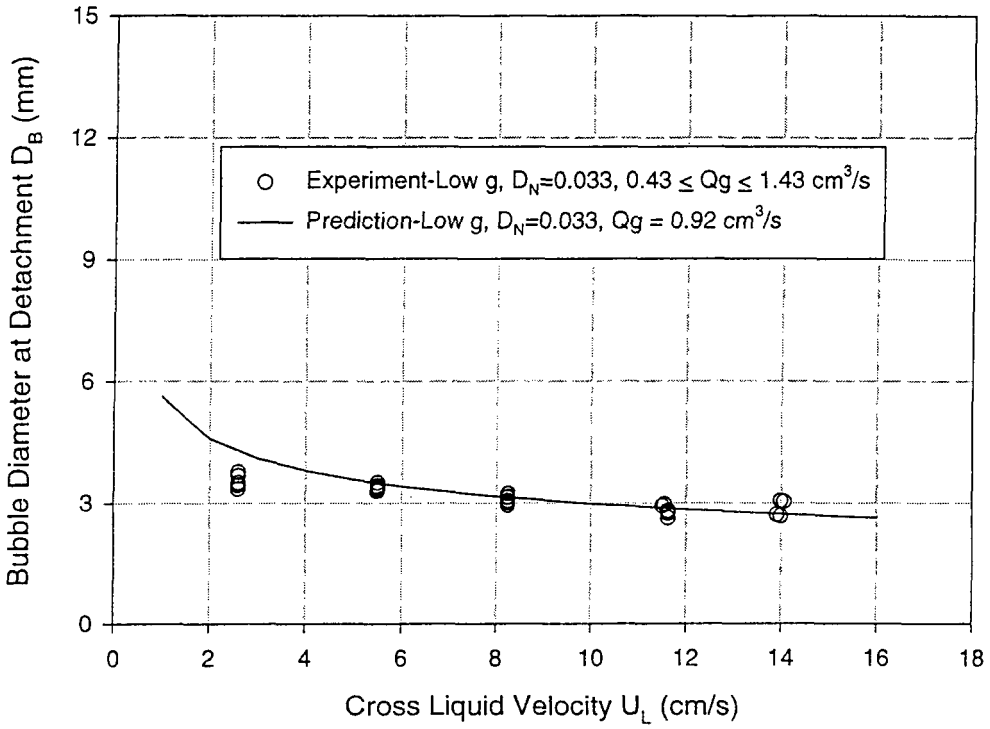

Figure 8. Bubble diameter at detachment as a function of the cross liquid velocity for D_N=0.033 cm and Q_g=0.92 cm^3/s.

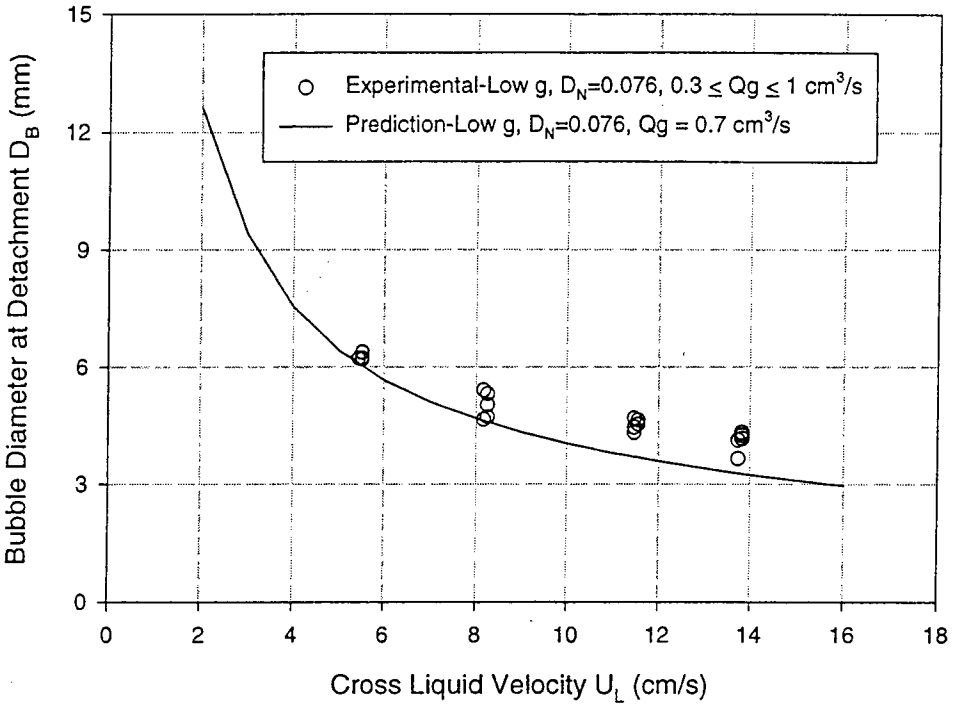

Figure 9. Bubble diameter at detachment as a function of the cross liquid velocity for D_N=0.076 cm and Q_g=0.7 cm^3/s.

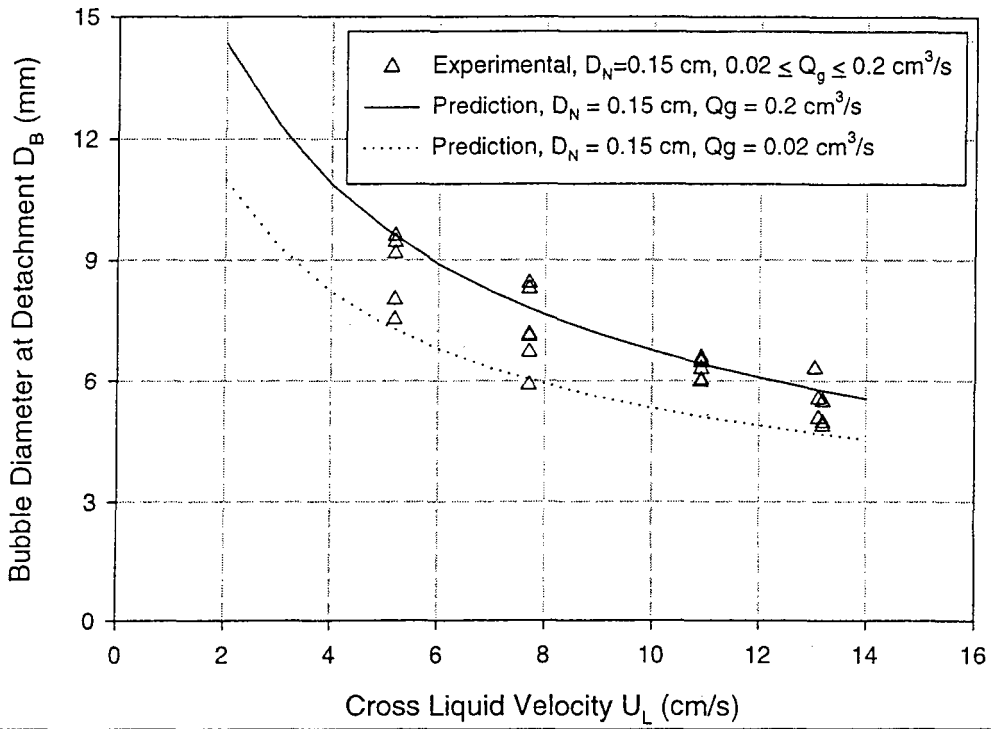

Figure 10. Bubble diameter at detachment as a function of the cross liquid velocity for D_N=0.15 cm and Q_g=0.2 and 0.02 cm^3/s.

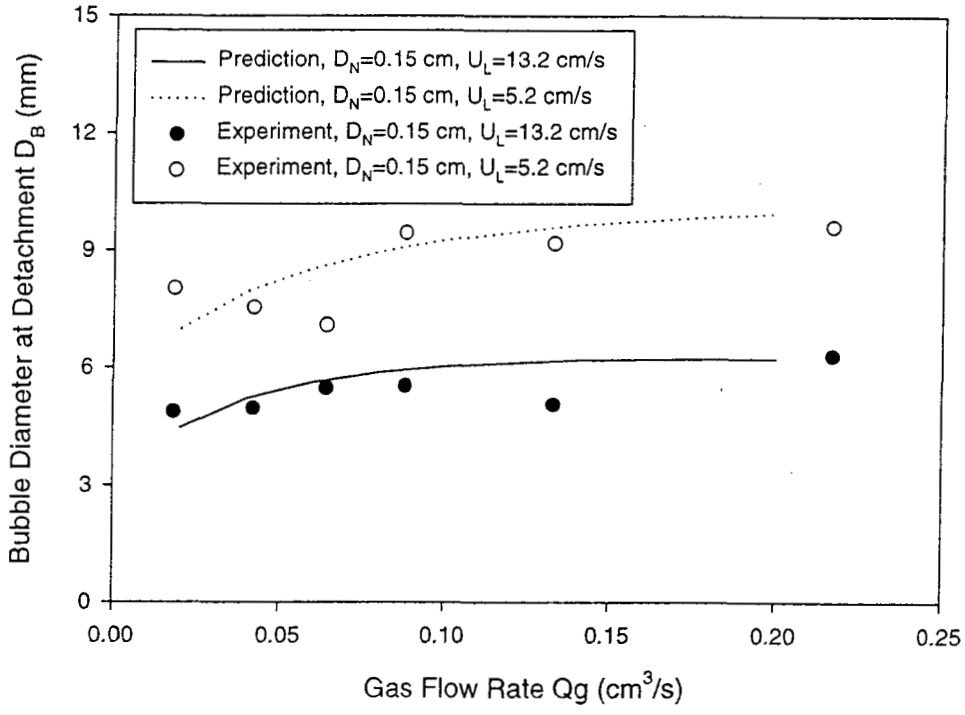

Figure 11. Bubble diameter at detachment as a function of gas flow rate for D_N=0.15 cm and U_L=13.2 and 5.2 cm/s. The lower set of data points corresponds to U_L=13.2 cm/s.

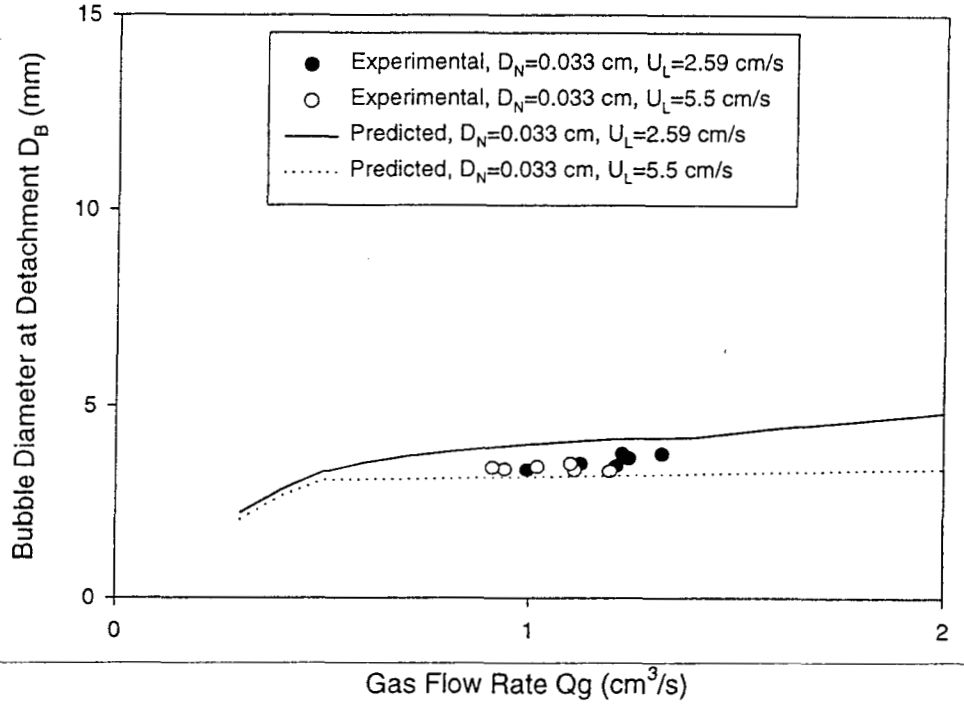

Figure 12. Bubble diameter at detachment as a function of gas flow rate for D_N=0.033 cm and U_L=2.9 and 5.5 cm/s

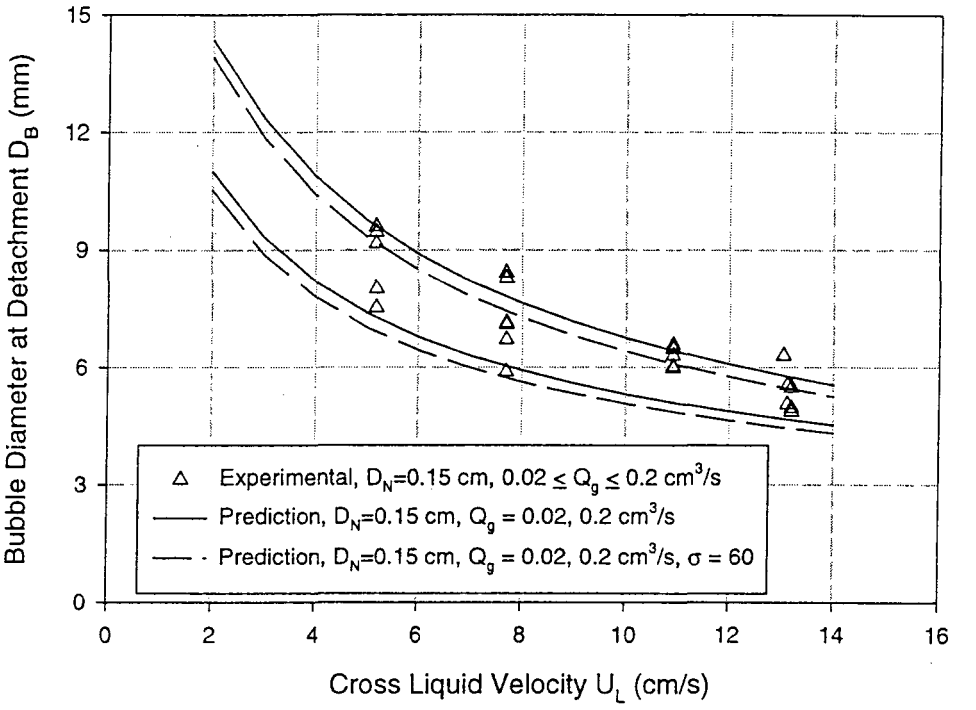

Figure 13. Predicted effects of the surface tension coefficient on the bubble diameter at detachment for D_N=0.15 cm.

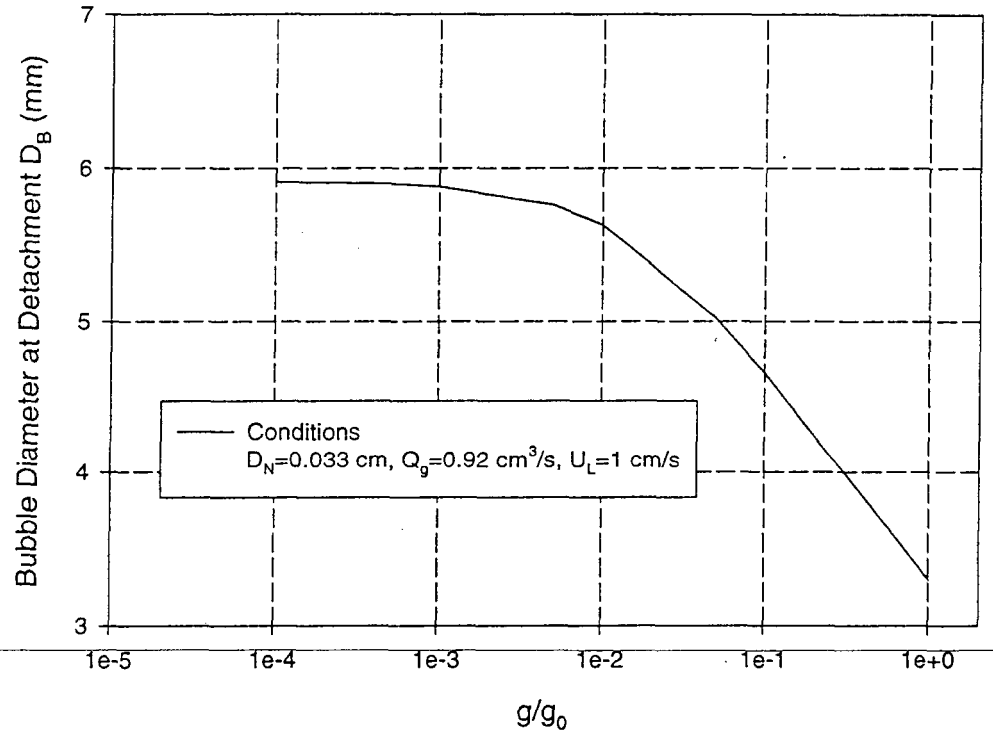

Figure 14. Bubble diameter as a function of the gravity levels for D_N=0.033 cm, Q_g=0.92 cm^3/s, and U_L=1 cm/s.

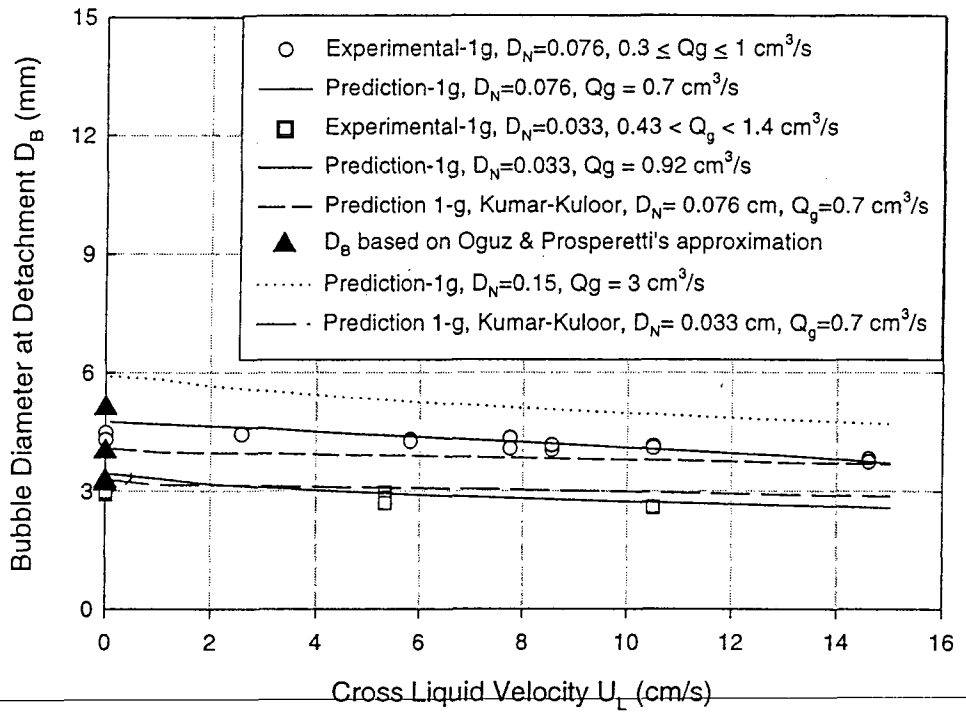

Figure 15. Predicted and experimental bubble diameter at detachment for normal gravity condition.